This is the accepted manuscript made available via CHORUS. The article has been published as:

Entangling-gate error from coherently displaced motional modes of trapped ions

B. P. Ruzic, T. A. Barrick, J. D. Hunker, R. J. Law, B. K. McFarland, H. J. McGuinness, L. P. Parazzoli, J. D. Sterk, J. W. Van Der Wall, and D. Stick

Phys. Rev. A **105**, 052409 — Published 5 May 2022

DOI: 10.1103/PhysRevA.105.052409

Entangling-gate error from coherently displaced motional modes of trapped ions

B. P. Ruzic,* T. A. Barrick, J. D. Hunker, R. J. Law, B. K. McFarland, H. J. McGuinness, L. P. Parazzoli, J. D. Sterk, J. W. Van Der Wall, and D. Stick
Sandia National Laboratories, Albuquerque, New Mexico 87185, USA
(Dated: April 20, 2022)

Entangling gates in trapped-ion quantum computers are most often applied to stationary ions with initial motional distributions that are thermal and close to the ground state, while those demonstrations that involve transport generally use sympathetic cooling to re-initialize the motional state prior to applying a gate. Future systems with more ions, however, will face greater non-thermal excitation due to increased amounts of ion transport and exacerbated by longer operational times and variations over the trap array. In addition, pre-gate sympathetic cooling may be limited due to time costs and laser access constraints. In this paper, we analyze the impact of such coherent motional excitation on entangling-gate error by performing simulations of Mølmer-Sørenson (MS) gates on a pair of trapped-ion qubits with both thermal and coherent excitation present in a shared motional mode at the start of the gate. We quantify how a small amount of coherent displacement erodes gate performance in the presence of experimental noise, and we demonstrate that adjusting the relative phase between the initial coherent displacement and the displacement induced by the gate or using Walsh modulation can suppress this error. We then use experimental data from transported ions to analyze the impact of coherent displacement on MS-gate error under realistic conditions.

I. INTRODUCTION

The ability to achieve precise control of qubits in the presence of noise is fundamental to the progress of quantum computation and quantum sensing. The Mølmer-Sørenson (MS) two-qubit entangling gate [1] for trapped-ion quantum computation is a good example of this built-in robustness, as the gate is designed to reduce the error caused by initial ion motion. While trapped-ion qubits encode quantum information in long-lived internal states, ion motion mediates the interactions between qubits, and noise that affects the quantized motional state can significantly degrade the performance of entangling gates. The use of a noisy degree of freedom to mediate two-qubit interactions is not unique to trapped-ion systems; for instance, entangling gates in neutral-atom systems employ a short-lived Rydberg state for this purpose [2]. Motional excitation also plays a critical role in quantum-sensing applications, including trapped-ion motional sensors [3] and inertially-sensitive neutral-atom interferometers, for which motional noise that persists after state preparation is predicted to be one of the dominant error sources [4].

A significant amount of research in trapped-ion quantum computation has focused on reducing the electric-field noise that causes "anomalous heating" [5, 6] and degrades MS-gate performance. The gate error results from incoherent excitation of the motional state both during the gate, while temporarily entangled with the internal-state qubit, and prior to the gate, by corrupting the initial motional state. For experiments that perform limited transport and/or sympathetically cool the ions prior to gates [7, 8], reference [9] accurately predicts the gate error because the ions are close to their motional ground state and thermal excitation contributes the majority of motion-related error.

This picture grows significantly more complicated for large trapped-ion systems that rely on extensive shuttling operations. This is particularly true for the quantum charge coupled device (QCCD) architecture [10], where experiments motivated by this concept have demonstrated linear [11], split/join [12, 13], and junction [14, 15] transport in both surface and 3D traps. Motional excitation over the course of an algorithm, whether from persistent voltage noise (i.e. anomalous heating) or transport induced excitation, is especially damaging to entangling-gate performance because each gate is sensitive to the accumulated excitation. A promising mitigation strategy relies on sympathetically cooling the motional degrees of freedom of the qubits while preserving any encoded quantum information [16], but this is costly in both time and infrastructure. Considerable time would be saved if sympathetic cooling were only needed occasionally to reduce small amounts of excitation. Similarly, the laser delivery infrastructure could be reduced if sympathetic cooling was only needed at a subset of sites.

In the work described here, we seek to better understand the impact of motional excitation on MS gates by computing the gate error that arises from both coherent and thermal excitation in the initial state of the gate-mediating motional mode. Both types of motion can arise from or be influenced by environmental and control sources, and while they do not affect the internal qubit directly, their accumulated impact prior to the two-qubit gate degrades its performance through temporary spin-motion entanglement. In particular, we investigate how each type of motion differently exacerbates the gate error resulting from fluctuations in the motional frequency, a ubiquitous source of experimental noise.

Imperfections in transport control inevitably lead to

* bruzic@sandia.gov

some degree of motional excitation, but careful control design can tilt the balance between thermal excitation and coherent displacement. For example, slow transport speeds can result in less coherent displacement after transport but contribute to longer operational times that introduce more anomalous heating. Additionally, background electric fields can drift over minutes and hours, altering the ion trajectory [12] and increasing the magnitude of induced coherent displacement over time. By analyzing our simulations of MS-gate error, we find that a small amount of coherent displacement at the start of the gate leads to a large error, with a strong dependence on the phase of the coherent displacement. While optimizing this phase provides robustness to coherent motional excitation, we find that implementing a first-order Walsh modulation greatly enhances this robustness and eliminates the phase dependence. We then apply our simulations to experimental data in which the application of a background electric field coherently displaces the motional modes of an ion.

II. MS-GATE MODEL

We model the application of an MS gate on two ions that are part of a linear chain of ions in a surface trap using the Hamiltonian,

$$H(t) = -\eta\Omega J_y \left(a e^{i\delta t} + a^\dagger e^{-i\delta t}\right), \tag{1}$$

which is in a rotating frame with respect to the atomic and trap degrees of freedom. The collective spin operator J_y has the form: $J_y = (\sigma_{y1} + \sigma_{y2})/2$, where σ_{yj} is the y Pauli spin operator for the j-th ion targeted by the gate. The Lamb-Dicke parameter η is the same for both ions, and Ω is the Rabi rate of the carrier transition for both ions. The operators $a^\dagger$ and a are the raising and lowering operators, respectively, for a harmonic oscillator that represents a single motional mode of the ion chain with angular frequency ν. During the gate, a dual-tone laser illuminates the ions with detunings $\pm\delta = \pm(\delta_c - \nu)$ from their blue and red motional sideband transitions, respectively, where the parameter δ_c is the detuning of the blue-detuned laser tone from the carrier transition. For simplicity, we have made the Lamb-Dicke approximation: $e^{i\eta(a+a^\dagger)} \approx 1 + i\eta(a+a^\dagger)$. We have also neglected the carrier transition, the far-off-resonant sideband transitions, and all other motional modes.

The exact analytic solution for the propagator $U(t)$ is,

$$U(t) = e^{-i\mathcal{B}(t)J_y^2} D(J_y\alpha(t)),$$
$$\mathcal{B}(t) = \frac{i}{2}\int_0^t \left(\frac{\mathrm{d}\alpha(t')}{\mathrm{d}t'}\alpha^*(t') - \alpha(t')\frac{\mathrm{d}\alpha^*(t')}{\mathrm{d}t'}\right)\mathrm{d}t', \tag{2}$$

which is equivalent to the solution in reference [9]. The displacement operator $D(J_y\alpha(t)) = \exp\left[J_y(\alpha(t)a^\dagger - \alpha^*(t)a)\right]$ is conditioned on the spin state of the targeted ions, and $\alpha(t)$ describes the phase-space trajectory of the ion chain. The phase $\mathcal{B}(t)$, which governs the amount of spin entanglement accrued during the gate, is real and positive (negative) for clockwise (counter-clockwise) trajectories. In terms of the parameters of $H(t)$,

$$\alpha(t) = \frac{\eta\Omega}{\delta}\left(1 - e^{-i\delta t}\right),$$
$$\mathcal{B}(t) = \frac{\eta^2\Omega^2}{\delta^2}\left(\delta t - \sin\delta t\right). \tag{3}$$

To simulate the MS gate, we use $U(t)$ to propagate the density matrix of the ions $\rho(t)$ from their initial state,

$$\rho(0) = \rho_{\mathrm{spin}} \otimes \rho_{\mathrm{motion}}, \tag{4}$$

where ρ_{spin} and ρ_{motion} describe the initial spin and motional degrees of freedom, respectively, to the state $\rho(\tau)$ at the end of the gate. The error of this gate depends on the character of the initial motional state ρ_{motion}, which accumulates all prior motional excitation since the ions were last cooled, including excitation from gates, heating, and transport.

III. INITIAL MOTIONAL STATE

The experimental realization of a quantum algorithm on a linear chain of ions can incur both coherent and incoherent motional excitation, which we represent as a coherent displacement in phase space $\alpha = |\alpha|e^{i\phi}$ and an increase in the ion temperature T, respectively. Under this premise, an ion chain cooled to its motional ground state at the start of the algorithm arrives in a thermal mixture of coherently displaced Fock states immediately before an MS gate occurs. We represent the n-th Fock state of the harmonic oscillator by $|n\rangle$, and we represent a coherently displaced Fock state by,

$$|\alpha, n\rangle = D(\alpha)\,|n\rangle, \tag{5}$$

where $D(\alpha) = \exp\left(\alpha a^\dagger - \alpha^* a\right)$ is the displacement operator. Hence, we describe the initial motional state for the gate by the partial density matrix,

$$\rho_{\mathrm{motion}} = \sum_{n=0}^{\infty} \frac{1}{1+\bar{n}_{\mathrm{th}}}\left(\frac{\bar{n}_{\mathrm{th}}}{1+\bar{n}_{\mathrm{th}}}\right)^n |\alpha, n\rangle\langle\alpha, n|, \tag{6}$$

where $\bar{n}_{\mathrm{th}} = (\exp(\hbar\nu/k_{\mathrm{B}}T) - 1)^{-1}$ in which k_{B} is the Boltzmann constant.

The coherently displaced Fock state $|\alpha, n\rangle$ has the following expansion onto Fock states [17],

$$|\alpha, n\rangle = \sum_{m=0}^{\infty} C_m^{(\alpha,n)}\,|m\rangle,$$
$$C_m^{(\alpha,n)} = e^{-|\alpha|^2/2}\sqrt{n!/m!}\,\alpha^{m-n} L_n^{(m-n)}(|\alpha|^2), \tag{7}$$

where $L_n^{(m-n)}$ is the generalized n-th order Laguerre polynomial. The expectation value of the number operator $\hat{n} = a^\dagger a$ in the state ρ_{motion} is $\langle\hat{n}\rangle = |\alpha|^2 + \bar{n}_{\mathrm{th}}$, and this quantity determines the average motional energy $\hbar\nu(1/2+\langle\hat{n}\rangle)$. Even though $\langle\hat{n}\rangle$ contains equal contributions from $|\alpha|^2$ and $\bar{n}_{\rm th}$, coherent displacement generates correlations between different Fock states and, in this way, produces a fundamentally different motional state than thermal excitation.

When the ion chain is coherently displaced prior to the gate, $\alpha \neq 0$, the operator $D(J_y\alpha(t))$ from equation (2) imparts an additional spin-dependent phase shift on the ions from the non-additive property of coherent displacements,

$$D\left(J_y\alpha'(t)\right)D\left(\alpha\right) = e^{J_y(\alpha'(t)\alpha^* - \alpha'^*(t)\alpha)/2} D\left(J_y\alpha'(t)+\alpha\right). \tag{8}$$

Using our expression for $\alpha(t)$ from equation (3), we obtain,

$$\alpha'(t)\alpha^* - \alpha'^*(t)\alpha = \frac{2i\eta\Omega|\alpha|}{\delta}\left(\sin(\delta t+\phi)-\sin(\phi)\right). \tag{9}$$

Therefore, when $\alpha \neq 0$ and $\delta t \neq 2\pi k$, where k is an integer, the MS-gate produces an additional J_y rotation that depends on ϕ.

IV. MS-GATE ERROR

We quantify the error of the MS gate by computing both its entanglement infidelity ϵ_e [18] and diamond error $\epsilon_\diamond$ [19]. The entanglement infidelity quantifies the performance of the gate averaged over input states, and the diamond error assesses the worst-case performance of the gate for all possible measurements and initial states. Both metrics depend linearly on the amount of stochastic error, and they are equal when the gate error is purely stochastic. While coherent errors affect $\epsilon_\diamond$ linearly, ϵ_e depends quadratically on coherent error [20]. As a result, $\epsilon_\diamond$ can be much larger than ϵ_e when the gate error is small and predominantly coherent. By using both metrics, one can assess at a glance the relative importance of stochastic vs. coherent errors in the gate. For our purposes, any difference between the two metrics can signal the presence of a coherent error. If the two metrics are very close, the gate error is likely dominated by stochastic error.

While the initial motional-state distribution affects the gate error associated with multiple control errors, we focus on the interplay between this distribution and motional frequency fluctuations because of their relatively large impact on gate performance compared to other control errors (e.g. laser intensity drift) and because the same physical noise sources (e.g. background electric fields and imperfect control voltages) contribute to both quantities. We consider different values of the initial phase ϕ of the coherent state prior to the gate, and we quantify the error after employing first-order Walsh modulation [21].

Although our MS-gate model is appropriate for a wide range of experimental conditions, we provide a concrete example by simulating an MS gate designed to complete $K = 2$ counter-clockwise loops in phase space during a gate duration of $\tau = 60$ μs. This requires $\delta/2\pi = -K/\tau = -33.3$ kHz to close the loops and $\eta\Omega/2\pi = \sqrt{K}/2\tau = 11.8$ kHz to produce $\mathcal{B}(\tau) = -\pi/2$. We also choose the motional frequency $\nu/2\pi = 3$ MHz, which is a representative value for the axial, center-of-mass motional mode of a linear chain of $^{40}\mathrm{Ca}^+$ ions in a surface trap.

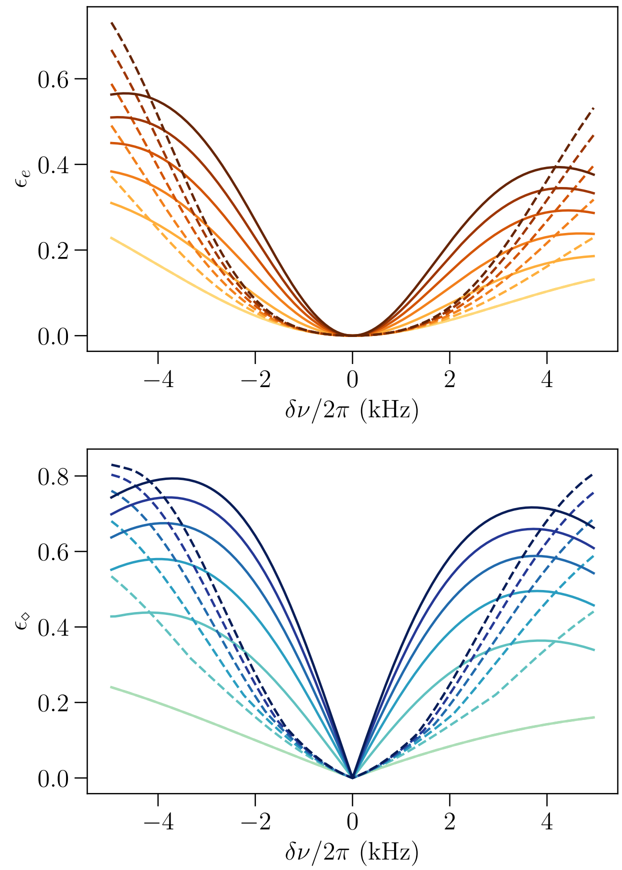

FIG. 1: Entanglement infidelity ϵ_e and diamond error $\epsilon_\diamond$ for an MS gate vs. motional frequency error $\delta\nu/2\pi$ with $\bar{n}_{\rm th} = 0$. From bottom (lightest) to top (darkest) in each plot, the calculations are for $|\alpha|^2 = 0$ to 2 in steps of 0.4 with $\phi = 0$ (solid lines) and with $\phi = \pi/2$ (dashed lines). For $|\alpha|^2 = 0$, the gate error is the same for both values of ϕ.

We incorporate motional frequency error into the MS-gate model by shifting ν: $\nu = \nu_0 + \delta\nu$, where $\nu_0/2\pi = 3$ MHz. This causes δ to deviate from its optimal value: $\delta = \delta_0 - \delta\nu$, where $\delta_0/2\pi = -33.3$ kHz, while τ remains fixed. We consider values of $|\delta\nu|/2\pi \lesssim 5$ kHz, which can have a substantial effect on δ, but we neglect the effect $\delta\nu$ has on η because $\delta\nu \ll \nu_0$. In this approximation, $\delta\nu$ only influences gate dynamics through its effect on δ. This detuning error prevents the phase-space trajectory from closing at the end of the gate, and from equation (9), we see that the magnitude of the additional J_y rotation that occurs when both $\delta t \neq 2\pi k$ and $\alpha \neq 0$ depends on ϕ. By substituting $t = \tau$ and $\delta = \delta_0 - \delta_\nu$ into this equation and expanding the right-hand-side for small δ_ν, we find,

$$\alpha'(\tau)\alpha^* - \alpha'^*(\tau)\alpha \approx \frac{-2i\eta\Omega|\alpha|}{\delta_0} \times \left(\cos\phi\,\delta_\nu\tau + \left(\frac{\cos\phi}{\delta_0\tau} + \frac{\sin\phi}{2}\right)\delta_\nu^2\tau^2\right). \tag{10}$$

From this equation, we see that setting $\phi = \pi/2 + \pi n$, where n is an integer, eliminates the first-order contribution to the additional J_y rotation from δ_ν.

Fig. 1 shows how the simulated MS-gate entanglement infidelity ϵ_e and diamond error $\epsilon_\diamond$ depend on the motional frequency error $\delta\nu/2\pi$ for several values of $|\alpha|^2$ with $\bar{n}_{\text{th}} = 0$, for both $\phi = 0$ and $\phi = \pi/2$. For $|\delta\nu|/2\pi \lesssim 3$ kHz, the gate error grows as the magnitude of motional frequency error increases. For $|\delta\nu|/2\pi \gtrsim 3$ kHz, the gate error oscillates and remains large. An experiment would observe these features if the motional frequency drifts away from $\nu_0/2\pi$ over the course of many experiments. The gate error is more sensitive to $\delta\nu$ for higher values of $|\alpha|^2$, and this sensitivity depends on ϕ. Hence, for a certain acceptable gate error, the values of ϕ and $|\alpha|^2$ set the time between necessary re-calibrations of ν.

As shown in Fig. 1, significant motional frequency error ($|\delta\nu|/2\pi = 3$ to 5 kHz) and only modest coherent displacement ($|\alpha|^2 = 0.4$ to 2) generates a large gate error that is comparable for both $\phi = 0$ and $\phi = \pi/2$. However, for values of $\delta\nu$ that produce experimentally relevant gate errors, coherent states with $\phi = \pi/2$ show a significant reduction in the sensitivity of gate error to $\delta\nu$, as compared to $\phi = 0$. For example, with $\delta\nu/2\pi = -600$ Hz and $|\alpha|^2 = 2$, $\epsilon_e = 0.030$ (0.0045) and $\epsilon_\diamond = 0.23$ (0.042) for $\phi = 0$ ($\pi/2$). We also note that initial states with phase $\phi + \pi n$, where n is an integer, incur the same gate error.

In addition to drifting over the course of many experiments, the motional frequency fluctuates from shot to shot during a single experiment due to voltage noise on the electrodes and other sources. We model this kind of noise by averaging the MS gate over a Gaussian distribution of motional frequencies with width $\sigma/2\pi$ and centered at $\nu_0/2\pi = 3$ MHz. Fig. 2 shows how the entanglement infidelity ϵ_e and the diamond error $\epsilon_\diamond$ of the average MS gate depend on ϕ when $\sigma/2\pi = 600$ Hz. Although significantly lower frequency variations have been measured [22, 23], this value of $\sigma/2\pi$ is representative of motional frequency fluctuations measured in several surface traps operated at Sandia. Additionally, aspects of larger ion trap arrays will increase the variation in motional frequencies; these include more neighboring electrodes, electrical component variation, greater laser power above the trap surface, and dielectric exposure due to integrated optics.

From Fig. 2 we see that $\phi = \pi/2$ provides maximum robustness to motional frequency noise when $\sigma/2\pi = 600$ Hz. The entanglement infidelity ϵ_e has a dramatic minimum at $\phi = \pi/2$. Although the minimum of $\epsilon_\diamond$ is not exactly at $\phi = \pi/2$, this value of ϕ is in the center of an approximately flat region of $\epsilon_\diamond$ vs. ϕ, and ϕ itself can be altered by motional frequency noise. While the increase of both error metrics with $|\alpha|^2$ is significantly suppressed at $\phi = \pi/2$, their increase with $\bar{n}_{\text{th}}$ shows only a small variation with ϕ.

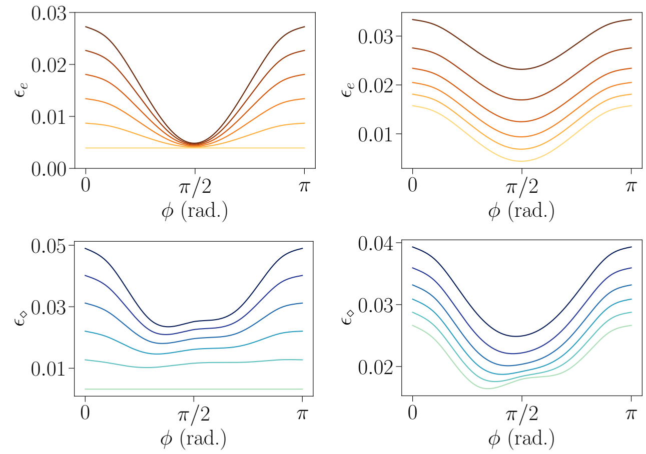

(a) (b)

FIG. 2: Entanglement infidelity ϵ_e and diamond error $\epsilon_\diamond$ for an MS gate averaged over a Gaussian distribution of motional frequencies with width $\sigma/2\pi = 600$ Hz and centered at $\nu_0/2\pi = 3$ MHz vs. the phase ϕ of the initial coherent state. From bottom (lightest) to top (darkest) in each plot, the calculations are for (a) $|\alpha|^2 = 0$ to 2 in steps of 0.4 with $\bar{n}_{\text{th}} = 0$ and for (b) $\bar{n}_{\text{th}} = 0$ to 2 in steps of 0.4 with $|\alpha|^2 = 1$.

To demonstrate the effect of changing ϕ from 0 to $\pi/2$, we provide the following example. With $\sigma/2\pi = 600$ Hz, $\bar{n}_{\text{th}} = 0$, and $|\alpha|^2 = 2$, $\epsilon_e = 0.027$ (0.0048) and $\epsilon_\diamond = 0.049$ (0.025) at $\phi = 0$ ($\pi/2$). This corresponds to an 82% reduction in ϵ_e and a 49% reduction in $\epsilon_\diamond$. We also note that the minimum in the gate error at $\phi = \pi/2$ becomes slightly more pronounced for smaller values of σ. For example, when $\sigma/2\pi = 200$ Hz, changing ϕ from 0 to $\pi/2$ corresponds to an 86% reduction in ϵ_e and a 52% reduction in $\epsilon_\diamond$. For $\sigma/2\pi \gtrsim 600$ Hz, the minimum ϵ_e remains at $\phi = \pi/2$, and two minima emerge in $\epsilon_\diamond$ vs. ϕ.

The sensitivity of transport to experimental conditions like electrode voltages, filters, and relative timing of pulses prevents the calculation of ϕ *a priori*. However, by providing a time delay after transport, one can vary the value of ϕ at the start of the gate and minimize ϵ_e to select $\phi = \pi/2 + n\pi$. Alternatively, one can minimize ϵ_e by varying the phase of the gate displacement: $\alpha(t) \rightarrow \alpha(t)e^{i\theta}$, where θ is equal to half the relative phase between the blue-detuned and red-detuned laser tones: $\theta = (\phi_{\text{b}} - \phi_{\text{r}})/2$, which is set to zero in equation (1). From equations (2) and (8), it is straightforward

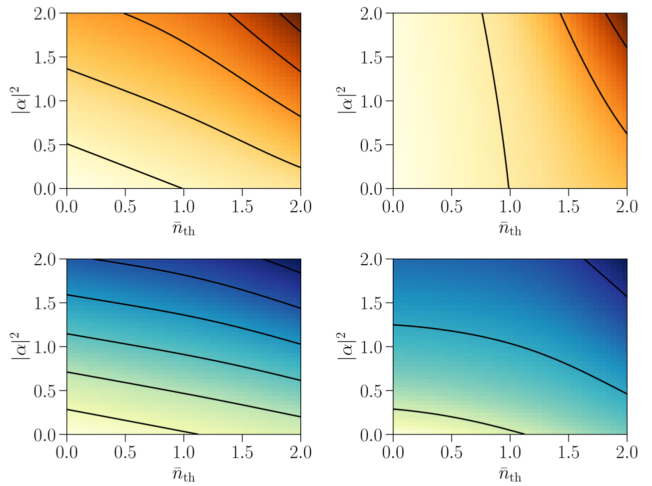

(a) (b)

FIG. 3: (upper plots) Entanglement infidelity ϵ_e and (lower plots) diamond error $\epsilon_\diamond$ for an MS gate averaged over a Gaussian distribution of motional frequencies with width $\sigma/2\pi = 600$ Hz and centered at $\nu_0/2\pi = 3$ MHz vs. $|\alpha|^2$ and $\bar{n}_{\text{th}}$, for (a) $\phi = 0$ and for (b) $\phi = \pi/2$. In each plot, the color represents increasing gate error from lightest to darkest, and the contours start at 0.01 and increase in steps of 0.01 from the lower-left to the upper-right.

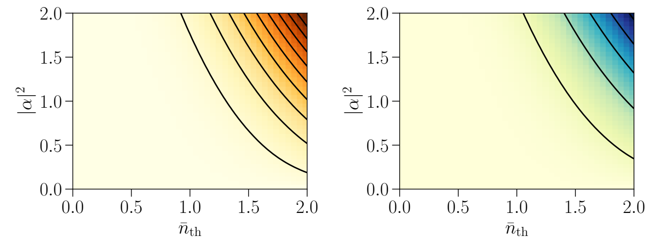

(a) (b)

FIG. 4: (a) Entanglement infidelity ϵ_e and (b) diamond error $\epsilon_\diamond$ for an MS gate with first-order Walsh modulation averaged over a Gaussian distribution of motional frequencies with width $\sigma/2\pi = 600$ Hz and centered at $\nu_0/2\pi = 3$ MHz vs. $|\alpha|^2$ and $\bar{n}_{\text{th}}$. There is no dependence on ϕ. In each plot, the color represents increasing gate error from lightest to darkest, and the contours start at 0.002 and increase in steps of 0.002 from the lower-left to the upper-right.

to see that the gate error depends on ϕ and θ through only their difference. Therefore, instead of changing ϕ, one can vary θ to select $\phi - \theta = \pi/2 + n\pi$ and minimize ϵ_e. This method will likely be faster and achieve a more consistent value of $\phi - \theta$ than adding a time delay. For simplicity, we retain $\theta = 0$ throughout this paper, but the same results hold if we replace ϕ with $\phi - \theta$. Optimizing this relative phase will simultaneously minimize $\epsilon_\diamond$ and improve the performance of quantum algorithms that use these gates.

Fig. 2 shows that $\epsilon_\diamond$ is more sensitive than ϵ_e to coherent displacement. This is consistent with coherent displacement causing a substantial amount of coherent gate error, as opposed to the purely stochastic error caused by thermal excitation. As quantum circuits amplify coherent gate error, it is especially damaging to long quantum algorithms that involve many gates [24]. As a result, the balance between coherent displacement and thermal excitation plays a critical role in the design of transport solutions that maximize circuit performance, including the choice of transport speeds. Although this study focuses on motional frequency noise, other noise sources (e.g. uncontrolled ac-Stark shifts) may amplify the detrimental effect of coherent displacement on high-fidelity gates.

To better characterize the optimal balance between coherent displacement and thermal excitation prior to the gate, Fig. 3 shows how the entanglement infidelity ϵ_e and the diamond error $\epsilon_\diamond$ of an MS gate averaged over a Gaussian distribution of motional frequencies with width $\sigma/2\pi = 600$ Hz and centered at $\nu_0/2\pi = 3$ MHz depend on $|\alpha|^2$ and $\bar{n}_{\text{th}}$. For small magnitudes of coherent displacement ($|\alpha|^2 \lesssim 1$) and thermal excitation ($\bar{n}_{\text{th}} \lesssim 1$), these forms of motion make independent contributions to the gate error, but their independence breaks down for larger magnitudes. The gradient in these plots indicates that increasing either $|\alpha|^2$ or $\bar{n}_{\text{th}}$ leads to a higher gate error for all initial states. For $\phi = 0$, the gradient is larger in the $|\alpha|^2$ direction than in the $\bar{n}_{\text{th}}$ direction, indicating that a coherent displacement prior to the gate is more detrimental than thermal excitation of the same average energy to gate performance. It therefore can be worthwhile to seek transport solutions which reduce the amount of coherent displacement, even at the expense of additional thermal excitation due to longer transport times, when $\phi = 0$.

However, when $\phi = \pi/2$, the gradient of ϵ_e is much larger in the $\bar{n}_{\text{th}}$ direction than in the $|\alpha|^2$ direction, even though the gradient of $\epsilon_\diamond$ is still larger in the $|\alpha|^2$ direction. This implies that the optimal transport solution depends on the application. One can increase the speed of transport to minimize thermal excitation prior to the gate and reduce ϵ_e, but the trade-off in increased coherent displacement will raise $\epsilon_\diamond$ and degrade the performance of some quantum algorithms.

While optimizing ϕ reduces gate error caused by the initial motion of the ions, the residual gate error may still be unacceptable for certain applications. To address this situation, we also study MS-gate errors while implementing a first-order Walsh modulation in our simulations. The modulated gate can be accomplished by setting half the sum of the phases of the two laser tones $(\phi_{\text{b}} + \phi_{\text{r}})/2$ to zero, as it is in equation (1), for the first half of the gate ($t < \tau/2$) and then shifting this phase to π for the rest of the gate ($t \geq \tau/2$). This amounts to flipping the sign of the Hamiltonian H halfway through the gate: $H(t \geq \tau/2) = -H(t < \tau/2)$ [21].

Fig. 4 shows how the entanglement infidelity ϵ_e and the diamond error $\epsilon_\diamond$ of an MS gate with first-order Walsh modulation averaged over a Gaussian distribution of motional frequencies with width $\sigma/2\pi = 600$ Hz and centered at $\nu_0/2\pi = 3$ MHz depend on $|\alpha|^2$ and $\bar{n}_{\rm th}$. We can see that the modulation gives the gate a strong robustness to motional frequency noise as the error magnitudes are much smaller than without Walsh modulation. In addition, the modulated gates are strongly robust to the exacerbating effect of the initial motional distribution. For $|\alpha|^2 = 0$ ($\bar{n}_{\rm th} = 0$) the gate error is independent of $\bar{n}_{\rm th}$ ($|\alpha|^2$), and only the combination of these two forms of motional excitation reduce gate performance compared to the motional ground state. The gate error is also independent of ϕ.

Although Walsh modulation reduces the gate error from residual ion motion after transport, implementing this technique may not be ideal for every situation. Walsh modulation requires the ion chain to traverse at least two loops in phase space ($k = 2$), and the required gate duration increases with the number of loops for a fixed laser power: $\tau = \pi\sqrt{k}/\eta\Omega$, increasing the gate duration by at least a factor of $\sqrt{2}$ from its minimum. If the gate is dominated by incoherent errors that accrue during the gate (e.g. anomalous heating), implementing Walsh modulation can decrease the overall gate performance.

V. TRANSPORT MEASUREMENTS

To predict realistic magnitudes of MS-gate error due to small amounts of motional excitation, we apply our simulations to experimentally measured motional spectra of excited Fock states after linear transport. This matches a relevant operational scenario for a trapped-ion quantum computer using the QCCD architecture, in which transport is calibrated for low motional excitation but over time background electric fields arise and result in excess motional heating.

In our experiment, the ion is shuttled away and back to its initial position at 16 m/s, and a delay is added at the turn-around point to eliminate most coherent excitation. After shuttling, we collect blue-sideband Rabi-flopping data to determine the coherent and thermal populations of the transported ion [25]. Then we apply a controlled electric-field offset of $E_z = 40$ V/m in the axial direction to our optimized voltage solution to mimic a background electric field that would typically arise over the course of hours in an experiment, and we collect new blue-sideband Rabi-flopping data. Fig. 5 shows the experimental data, where each data point is an average of $M = 500$ shots in the experiment. The error bars shown in the figure represent the statistical uncertainty $\sqrt{P_e(1-P_e)/M}$ of sampling from a binomial distribution, where P_e is the excited-state probability.

We model the blue-sideband Rabi-flopping experiments by assuming ideal Rabi oscillations, except for the addition of a phenomenological decoherence rate

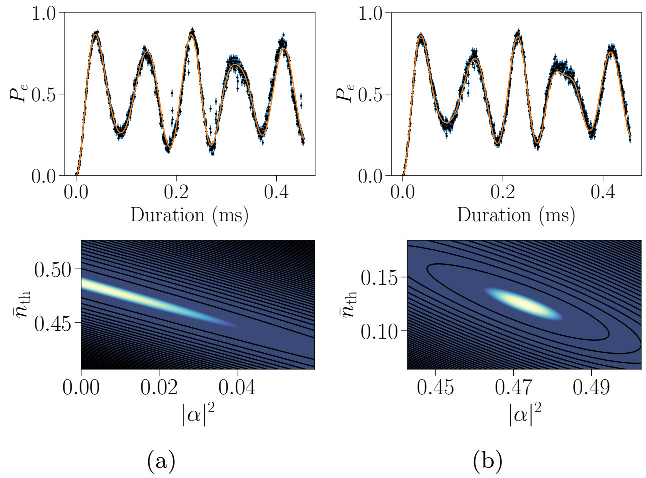

FIG. 5: Excited-state probability P_e during blue-sideband Rabi-flopping experiments and the log-likelihood vs. $|\alpha|^2$ and $\bar{n}_{\rm th}$ for (a) $E_z = 0$ and for (b) $E_z = 40$ V/m. In the upper plots, the black dots are the average of $M = 500$ measurements at each time step. The blue vertical line segments are the corresponding statistical error bars, and the orange line is the best-fit model of P_e based on a maximum likelihood estimation. In the lower plots, the color scales range from the maximum likelihood (lightest) to e^{-1} times the maximum likelihood (darkest), i.e., to one sigma. The black contours occur every five sigma.

$\gamma_n = \gamma_0(n+1)$ between $|n\rangle$ and $|n+1\rangle$. For this model, the excited-state probability P_e during the experiment has the form [26],

$$P_e = \frac{1}{2} - \frac{1}{2}\sum_{n=0}^{\infty} P_n \cos(2\Omega_{n,n+1}t)e^{-\gamma_n t}, \tag{11}$$

where $\Omega_{n,n+1} = \eta\Omega\sqrt{n+1}$ and $P_n = {\rm Tr}(\rho_{\rm motion}\,|n\rangle\langle n|)$.

Using the Rabi-flopping data shown in Fig. 5 for both $E_z = 0$ and $E_z = 40$ V/m, we perform a maximum likelihood estimation of the model parameters Ω, γ_0, $|\alpha|^2_0$, $\bar{n}_{\rm th,0}$, $|\alpha|^2_{40}$, and $\bar{n}_{\rm th,40}$. The additional subscript on $|\alpha|^2$ and $\bar{n}_{\rm th}$ denotes the value of E_z in V/m, and we demand that the parameters Ω and γ_0 are independent of E_z. Fig. 5 shows the values of P_e produced by the best-fit model. The relatively small number of outlying data points, which lie outside the statistical uncertainty of neighboring data points, has a negligible effect on the maximum likelihood estimation. We attribute the cause of the outlying data points to collisions or other catastrophic events that are not captured by the model.

The estimators for the model parameters are $\Omega/2\pi = 136$ kHz, $1/\gamma_0 = 1.34$ ms, $|\alpha|^2_0 = 0.00 \pm 0.04$, $\bar{n}_{\rm th,0} = 0.49 \pm 0.05$, $|\alpha|^2_{40} = 0.47 \pm 0.01$, and $\bar{n}_{\rm th,40} = 0.12 \pm 0.02$. We have determined the uncertainties by calculating the likelihood for the case of $E_z = 0$ and $E_z = 40$ V/m, separately, with Ω and γ_0 fixed at their optimal values. Fig. 5 shows contour plots of the log-likelihood vs. $|\alpha|^2$

and $\bar{n}_{\rm th}$. For $E_z = 40$ V/m, we define the uncertainty in each parameter to be half its maximum range on the curve defined by e^{-1} times the maximum likelihood. For $E_z = 0$, we define the uncertainty in each parameter to be its full range on this curve, noting that $|\alpha|_0^2$ is positive definite and that $\bar{n}_{\rm th,0}$ is highly unlikely to be this much greater than its optimal value. It is unclear why the thermal excitation is lower for $E_z = 40$ V/m; after measuring the excitation for multiple field offsets ranging from 0 to 40 V/m, we observed that the coherent excitation extracted from the fit increased monotonically with the amount of offset, but the thermal excitation behaved inconsistently.

We then use the estimators of $|\alpha|^2$ and $\bar{n}_{\rm th}$ to predict the MS-gate error after transport without implementing Walsh modulation. To represent the conditions of modern ion surface traps, we assume a Gaussian distribution of motional frequencies with width $\sigma/2\pi = 600$ Hz and centered at the optimal value of $\nu_0/2\pi = 3$ MHz. In this case, our simulations predict $\epsilon_e = 0.0069$ and $\epsilon_\diamond = 0.0061$ when $E_z = 0$. These values are independent of ϕ because $|\alpha|_0^2 = 0$. When $E_z = 40$ V/m, our simulations predict $\epsilon_e = 0.010$ (0.0049) and $\epsilon_\diamond = 0.015$ (0.013) for $\phi = 0$ ($\pi/2$). In this example, we see that a small background electric field of $E_z = 40$ V/m raises ϵ_e ($\epsilon_\diamond$) by 49% (150%) when $\phi = 0$, even though the field decreases $\bar{n}_{\rm th}$ by 0.37 and increases $|\alpha|^2$ by only 0.47, highlighting the sensitivity of MS-gate error to $|\alpha|^2$. When $\phi = \pi/2$, the 40 V/m field lowers ϵ_e by 29% – due to the decrease in $\bar{n}_{\rm th}$ and the relative insensitivity of ϵ_e to $|\alpha|^2$ – and raises $\epsilon_\diamond$ by 110%, which is 40% less than when $\phi = 0$.

This example demonstrates the benefits of optimizing ϕ after an experimental implementation of ion transport, but performing Walsh modulation can achieve greater error suppression in this case. From Fig. 4, we see that the Walsh-modulated gates achieve error rates well below 0.002 for both $E_z = 0$ and $E_z = 40$ V/m. While this study used linear ion transport, other types of transport are likely to cause greater magnitudes of coherent displacement for the same background electric field, further elevating the importance of reducing coherent displacement, optimizing ϕ, and implementing Walsh modulation.

VI. CONCLUSION

We have extended MS-gate models to include both coherent and thermal excitation of motional modes prior to the gate. We have demonstrated that small coherent displacements have a large impact on gate performance and generate significant coherent gate error, making this error source particularly detrimental to quantum algorithms that involve many gates and/or significant ion transport. Our simulations have focused on Gaussian-distributed motional frequency noise to provide a concrete example, but the interplay between coherent displacement and thermal excitation is important for a broad set of experimental realities with a diverse spectrum of both environmental and control-based noise sources. We have also validated our model of ion motion against measurements of the motional distribution after linear transport, and we have applied our simulations to predict MS-gate performance in a realistic experimental situation, with and without first-order Walsh modulation. As trapped-ion quantum processors scale up to larger numbers of qubits and support next-generation quantum algorithms, the analysis and methods presented in this paper will help maximize performance by assessing the trade-offs between operations that produce coherent and incoherent excitation of ion motion, a paradigm that is also relevant to other quantum-computing technologies and quantum sensors.

ACKNOWLEDGMENTS

We thank Kevin Young and Kenton Brown for fruitful discussions that helped guide this work. This research was funded by the U.S. Department of Energy, Office of Science, Office of Advanced Scientific Computing Research. Sandia National Laboratories is a multimission laboratory managed and operated by National Technology & Engineering Solutions of Sandia, LLC, a wholly owned subsidiary of Honeywell International Inc., for the U.S. Department of Energy's National Nuclear Security Administration under contract DE-NA0003525. This paper describes objective technical results and analysis. Any subjective views or opinions that might be expressed in the paper do not necessarily represent the views of the U.S. Department of Energy or the United States Government.

REFERENCES

[1] K. Mølmer and A. Sørensen, Phys. Rev. Lett. **82**, 1835 (1999).

[2] A. Mitra, M. J. Martin, G. W. Biedermann, A. M. Marino, P. M. Poggi, and I. H. Deutsch, Phys. Rev. A **101**, 030301 (2020).

[3] K. C. McCormick, J. Keller, S. C. Burd, D. J. Wineland, A. C. Wilson, and D. Leibfried, Nature **572**, 86 (2019).

[4] C. Brif, B. P. Ruzic, and G. W. Biedermann, PRX Quantum **1**, 010306 (2020).

[5] C. D. Bruzewicz, J. M. Sage, and J. Chiaverini, Phys. Rev. A **91**, 041402 (2015).

[6] I. A. Boldin, A. Kraft, and C. Wunderlich, Phys. Rev. Lett. **120**, 023201 (2018).

[7] Y. Wan, D. Kienzler, S. D. Erickson, K. H. Mayer, T. R. Tan, J. J. Wu, H. M. Vasconcelos, S. Glancy, E. Knill, D. J. Wineland, A. C. Wilson, and D. Leibfried, Science **364**, 875 (2019).

[8] J. M. Pino, J. M. Dreiling, C. Figgatt, J. P. Gaebler, S. A. Moses, M. S. Allman, C. H. Baldwin, M. Foss-Feig, D. Hayes, K. Mayer, C. Ryan-Anderson, and B. Neyenhuis, Nature **592**, 209 (2021).

[9] A. Sørensen and K. Mølmer, Phys. Rev. A **62**, 022311 (2000).

[10] D. Kielpinski, C. Monroe, and D. Wineland, Nature **417**, 709 (2002).

[11] A. Walther, F. Ziesel, T. Ruster, S. T. Dawkins, K. Ott, M. Hettrich, K. Singer, F. Schmidt-Kaler, and U. Poschinger, Phys. Rev. Lett. **109**, 080501 (2012).

[12] R. Bowler, J. Gaebler, Y. Lin, T. R. Tan, D. Hanneke, J. D. Jost, J. P. Home, D. Leibfried, and D. J. Wineland, Phys. Rev. Lett. **109**, 080502 (2012).

[13] M. Palmero, S. Martínez-Garaot, U. G. Poschinger, A. Ruschhaupt, and J. G. Muga, New Journal of Physics **17**, 093031 (2015).

[14] R. B. Blakestad, C. Ospelkaus, A. P. VanDevender, J. H. Wesenberg, M. J. Biercuk, D. Leibfried, and D. J. Wineland, Phys. Rev. A **84**, 032314 (2011).

[15] G. Shu, G. Vittorini, A. Buikema, C. S. Nichols, C. Volin, D. Stick, and K. R. Brown, Phys. Rev. A **89**, 062308 (2014).

[16] Y. Lin, J. P. Gaebler, T. R. Tan, R. Bowler, J. D. Jost, D. Leibfried, and D. J. Wineland, Phys. Rev. Lett. **110**, 153002 (2013).

[17] A. Wünsche, Quantum Optics **3**, 359 (1991).

[18] M. A. Nielsen, Physics Letters A **303**, 249 (2002).

[19] J. J. Wallman, Bounding experimental quantum error rates relative to fault-tolerant thresholds (2016), arXiv:1511.00727 [quant-ph].

[20] M. T. Mądzik, S. Asaad, A. Youssry, B. Joecker, K. M. Rudinger, E. Nielsen, K. C. Young, T. J. Proctor, A. D. Baczewski, A. Laucht, V. Schmitt, F. E. Hudson, K. M. Itoh, A. M. Jakob, B. C. Johnson, D. N. Jamieson, A. S. Dzurak, C. Ferrie, R. Blume-Kohout, and A. Morello, Nature **601**, 348 (2022).

[21] D. Hayes, S. M. Clark, S. Debnath, D. Hucul, I. V. Inlek, K. W. Lee, Q. Quraishi, and C. Monroe, Phys. Rev. Lett. **109**, 020503 (2012).

[22] T. P. Harty, M. A. Sepiol, D. T. C. Allcock, C. J. Ballance, J. E. Tarlton, and D. M. Lucas, Phys. Rev. Lett. **117**, 140501 (2016).

[23] R. Srinivas, S. C. Burd, H. M. Knaack, R. T. Sutherland, A. Kwiatkowski, S. Glancy, E. Knill, D. J. Wineland, D. Leibfried, A. C. Wilson, D. T. C. Allcock, and D. H. Slichter, Nature **597**, 209 (2021).

[24] J. K. Iverson and J. Preskill, New Journal of Physics **22**, 073066 (2020).

[25] D. Leibfried, D. M. Meekhof, B. E. King, C. Monroe, W. M. Itano, and D. J. Wineland, Phys. Rev. Lett. **77**, 4281 (1996).

[26] D. Leibfried, D. M. Meekhof, C. Monroe, B. E. King, W. M. Itano, and D. J. Wineland, Journal of Modern Optics **44**, 2485 (1997).